Smart Structures and Systems, *Vol. 34, No. 5 (2024) 283-297*
https://doi.org/10.12989/sss.2024.34.5.283

Smart Lyapunov LMI criterion for TMD RC structure systems via deep reinforcement learning algorithms

ZY Chen [1], Huakun Wu [2], Ruei-Yuan Wang[**1], Yahui Meng [1] and Timothy Chen[*3]

[1] *School of Science, Guangdong University of Petrochemical Technology, Maoming, Guangdong, China*
[2] *School of Computer Science, Guangdong Polytechnic Normal University, Guangzhou, Guangdong, China*
[3] *Division of Engineering and Applied Science, Caltech, CA 91125, USA*

(*Received December 12, 2023, Revised November 8, 2024, Accepted December 3, 2024*)

Abstract. This study presents a novel approach to enhancing the seismic performance of tuned mass damper (TMD) systems in reinforced concrete (RC) structures through the implementation of a Smart Lyapunov Linear Matrix Inequality (LMI) criterion, optimized via deep reinforcement learning (DRL) algorithms. Traditional methods for TMD design often rely on heuristic or empirical approaches, which may not adequately address the complexities of dynamic interactions in RC structures under varying seismic loads. By leveraging the capabilities of DRL, this research develops a framework that dynamically adjusts TMD parameters in real-time, ensuring optimal performance across a range of seismic scenarios. The proposed Smart Lyapunov LMI criterion provides a robust mathematical foundation for stability and performance assessment, allowing for the systematic evaluation of TMD effectiveness in mitigating structural vibrations. Through extensive numerical simulations, the integration of DRL algorithms demonstrates significant improvements in the adaptability and efficiency of TMD systems, outperforming conventional design methods. The results indicate that the proposed approach not only enhances the resilience of RC structures under seismic events but also contributes to the development of intelligent structural control systems. This research underscores the potential of combining advanced control theories with artificial intelligence techniques to address contemporary challenges in structural engineering, paving the way for more resilient and adaptive building designs in earthquake-prone regions.

Keywords: Deep Reinforcement Learning (DRL); fuzzy model; hybrid heuristic search algorithm; seismic performance, sustainable and resilience; vibration mitigation

1. Introduction

After an earthquake, structures will often be damaged. Therefore, damage analysis will be conducted on old structures after the disaster to determine the health status of the structures. In the past, visual inspection or destructive testing were mostly used, but these methods cannot accurately analyze structures and are also very uneconomical (Cai *et al*. 2022a, b, Zheng *et al*. 2022, 2023, Zhang 2023, Zhang *et al*. 2020, 2024a, b). With the advancement of the times, the development of non-destructive testing can effectively improve the original defect methods. Through instruments installed on structures, effective data can be observed, and appropriate structural parameters can be analyzed using physical meaning (Yao *et al*. 2022, Xu *et al*. 2022, Wu *et al*. 2023, Wang *et al*. 2024a, b, c, Jiang *et al*. 2024, Fan *et al*. 2024).

From this, we can infer the difference between the healthy state of the building and the state to be measured, and then obtain the structural safety state, which is called fundamental vibration analysis (e.g., Long *et al*. 2024a, b, Lin *et al*. 2024, Meng *et al*. 2023, 2024, Liu *et al*. 2024) and then identification or detection have been suggested in the literature. (e.g., Cheng *et al*. 2020, Chen *et al*. 2020, 2023 etc.). Non-destructive testing is a testing technology, also known as non-destructive testing, which means that the test object will not be damaged during testing, or that although it is damaged, it will not have a substantial impact on the nature of the product. Therefore, its testing is an effective tool to ensure the quality of structural materials and evaluate the service life of the structure.

The integration of advanced control strategies into structural engineering has garnered significant attention in recent years, particularly regarding the seismic performance of reinforced concrete (RC) structures. Among various control methods, tuned mass dampers (TMDs) have emerged as effective devices for mitigating vibrations induced by dynamic loads, such as earthquakes. The design and optimization of TMD systems are critical for enhancing the resilience of RC structures, and researchers have explored various methodologies to improve their effectiveness.

Tuned mass dampers are passive control devices consisting of a mass-spring-damper system strategically placed within a structure to counteract vibrations. The effectiveness of TMDs is highly dependent on their tuning parameters, including mass ratio, frequency, and damping characteristics. Traditional design approaches often rely on

*Corresponding author,
E-mail: t13929751005@gmail.com
**Co-corresponding author, Professor,
E-mail: rueiyuan@gmail.com

ISSN: 1738-1584 (Print), 1738-1991 (Online)

empirical formulas or heuristic methods, which may not adequately account for the complex interactions between the TMD and the primary structure (Zhu *et al*. 2024a, b). Recent studies have emphasized the need for more systematic design methodologies that can adapt to varying seismic conditions (Niu *et al*. 2022, Ni *et al*. 2024, Zhu *et al*. 2017, Zhang *et al*. 2020).

Lyapunov stability theory provides a robust framework for analyzing the stability of dynamic systems. The application of Lyapunov's direct method in structural control has been extensively explored, particularly through the formulation of Linear Matrix Inequalities (LMIs). LMIs serve as powerful tools for establishing stability criteria and optimizing control parameters (Yu *et al*. 2024, Shen *et al*. 2023, Toma and Chen 2024, Tian *et al*. 2024, Tan *et al*. 2023). Prior research has demonstrated that Lyapunov-based approaches can effectively ensure the stability of TMD systems when subjected to external disturbances, thereby enhancing the overall performance of RC structures (Zhou *et al*. 2020, Lu *et al*. 2017, 2019).

The advent of artificial intelligence, particularly deep reinforcement learning (DRL), has revolutionized the field of control systems. DRL algorithms enable systems to learn optimal control strategies through trial and error, allowing for real-time adaptation to changing conditions (Zhang *et al*. 2024c). In the context of structural engineering, DRL has been employed to optimize various control strategies, including active and semi-active control systems (Shu *et al*. 2025, Poudel and Bhandari 2023). This approach provides the capability to dynamically adjust TMD parameters in response to real-time seismic data, significantly improving the adaptability and effectiveness of vibration mitigation strategies.

Recent studies have begun to explore the synergy between Lyapunov stability criteria and DRL algorithms in the context of TMD systems. These investigations highlight the potential for developing intelligent control systems that leverage the strengths of both methodologies. For instance, researchers have proposed frameworks that utilize Lyapunov-based LMIs to guide the training of DRL agents, ensuring that learned policies adhere to stability constraints while optimizing performance (Li *et al*. 2024, Huang *et al*. 2023, 2024). This innovative approach not only enhances the design of TMDs but also contributes to the development of smart structural systems capable of responding to dynamic environmental conditions.

The literature indicates a growing interest in the integration of Smart Lyapunov LMI criteria with deep reinforcement learning algorithms for optimizing TMD systems in RC structures. This combination presents a promising avenue for enhancing seismic resilience through intelligent control strategies. As research continues to evolve, the potential for these methodologies to revolutionize structural engineering practices becomes increasingly evident, paving the way for more adaptive and resilient building designs in earthquake-prone regions. Future studies will be essential in validating these approaches and exploring their practical applications in real-world scenarios (Hao *et al*. 2022, Guan *et al*. 2024, Erum and Ahmad 2023, Chen *et al*. 2024a, b).

This study is organized as follows. First, a description of the system is presented. Then, based on the Lyapunov method, a stability criterion is derived to ensure asymptotic stability. Finally, a numerical example is given to demonstrate the results, and then conclusions are drawn to validate other control methods to be used. In addition, comparisons with numerical results are made to demonstrate its control performance.

2. Criteria and methods

A motion equation of any degree of freedom (DOF) nonlinear structure is shown as (Chen *et al*. 2023)

$$\mathbf{M}\ddot{\mathbf{x}}(t) + \mathbf{F}_c[\dot{\mathbf{x}}(t)] + \mathbf{F}_s[\mathbf{x}(t)] = \boldsymbol{\eta}^*\mathbf{f}^*(t) + \boldsymbol{\eta}\mathbf{f}(t) \quad (1)$$

in which $\mathbf{x}(t) = [x_1, x_2, \dots, x_m]^{\mathrm{T}} = m-$ displacement vector; $\mathbf{M} = (m \times m)$ matrix of mass: $\mathbf{F}_c[\mathbf{x}(t)]$ = m-damping vector of force; $\mathbf{F}_s[\mathbf{x}(t)]$ = m-stiffness vector of force; $\mathbf{f}^*(t) = [f_1^*(t), \dots, f_r^*(t)]^{\mathrm{T}}$ = r- unmeasured (or unknown) vector of excitation; $\boldsymbol{\eta}^* = (m \times r)$ matrix of excitation influence subjected to $\mathbf{f}^*(t)$; $\mathbf{f}(t) = [f_1(t), f_2(t), \dots, f_s(t)]^{\mathrm{T}}$ = s-measured (or known) vector of excitation; and $\boldsymbol{\eta} = (m \times s)$ matrix of citation influence subjected to $\mathbf{f}(t)$.We hereby have

$$\mathbf{Z}(t) = \left\{\mathbf{x}^{\mathrm{T}}, \dot{\mathbf{x}}^{\mathrm{T}}, \boldsymbol{\theta}^{\mathrm{T}}\right\}^{\mathrm{T}} \quad (2)$$

in which $\boldsymbol{\theta}^{\mathrm{T}} = [\theta_1, \theta_2, \dots, \theta_n]^{\mathrm{T}}$ means vector of parametric with θ_i $(i = 1,2, \dots, n)$ being the ith structure variable. Considering $\dot{\theta}_i = 0$ $(i = 1,2, \dots, n)$, i.e., the constants that one can get another transformation, i.e.

$$\dot{\mathbf{Z}}(t) = \mathbf{g}(\mathbf{Z}, \mathbf{f}, \mathbf{f} * t) + \mathbf{w}(t) \quad (3)$$

in which w(t) = model vector of noise (uncertainty) with $\mathbf{Q}(t)$. The observation is

$$\mathbf{y}_{k+1} = \mathbf{h}(\mathbf{Z}_{k+1}, \mathbf{f}_{k+1}, \mathbf{f}_{k+1}^*, k+1) + \mathbf{v}_{k+1} \quad (4)$$

in which $\mathbf{y}_{k+1}$ is an - measured (observation) vector of output at $t = (k+1)\Delta t$ (sampling time step Δt), i.e.., $\mathbf{y}_{k+1} = \mathbf{y}(t = (k+1)\Delta t), \mathbf{Z}_{k+1} = \mathbf{Z}(t = (k+1)\Delta t)$, $\mathbf{f}_{k+1} = \mathbf{f}(t = (k+1)\Delta t)$, and $\mathbf{f}_{k+1}^* = \mathbf{f}^*(t = (k+1)\Delta t)$. In Eq. (4), $\mathbf{v}_{k+1}$ is a measurement of noise to be a Gaussianwhite $E[\mathbf{v}_k\mathbf{v}_j^{\mathrm{T}}] = \mathbf{R}_k\delta_{kj}$.

Eqs. (3) and (4) are lincarized with respect to the estimates $\hat{\mathbf{Z}}_{k|k}$, $\hat{\mathbf{Z}}_{k+1|k}$ and $\hat{\mathbf{f}}_{k|k}^*$ as follows

$$\mathbf{g}_k \approx \hat{\mathbf{g}}_{k|k} + \mathbf{G}_{k|k}(\mathbf{Z}_k - \hat{\mathbf{Z}}_{k|k}) + \mathbf{B}_{k|k}^*(\mathbf{f}_k^* - \hat{\mathbf{f}}_{k|k}^*) \quad (5)$$

$$\begin{aligned}\mathbf{h}_{k+1} \approx \hat{\mathbf{h}}_{k+1|k} + \mathbf{H}_{k+1|k}\left(\mathbf{Z}_{k+1} - \hat{\mathbf{Z}}_{k+1|k}\right) \\ +\mathbf{D}_{k+1|k}^*(\mathbf{f}_{k+1}^* - \hat{\mathbf{f}}_{k|k}^*)\end{aligned} \quad (6)$$

Furthermore, we have $\mathbf{g}_k = \mathbf{g}(\mathbf{Z}_k, \mathbf{f}_k, \mathbf{f}_k^*, k\Delta t), \mathbf{h}_{k+1} = \mathbf{h}(\mathbf{Z}_{k+1}, \mathbf{f}_{k+1}, \mathbf{f}_{k+1}^*, k+1)$, $\hat{\mathbf{g}}_{k|k} = \mathbf{g}\left(\hat{\mathbf{Z}}_{k|k}, \mathbf{f}_k, \hat{\mathbf{f}}_{k|k}^*, k\Delta t\right)$, $\hat{\mathbf{h}}_{k+1|k} = \mathbf{h}(\hat{\mathbf{Z}}_{k+1|k}, \mathbf{f}_{k+1}, \hat{\mathbf{f}}_{k|k}^*, k+1)$, and

$$\mathbf{G}_{k|k} = [\partial \mathbf{g}_k / \partial \mathbf{Z}_k]_{\mathbf{Z}_k=\hat{\mathbf{Z}}_{k|k},\mathbf{f}_k^*=\hat{\mathbf{f}}_{k|k}^*} \quad (7)$$

$$\mathbf{B}_{k|k}^* = [\partial \mathbf{g}_k / \partial \mathbf{f}_k^*]_{\mathbf{Z}_k=\hat{\mathbf{Z}}_{kk},\mathbf{f}_k^*=\hat{\mathbf{f}}_{k|k}^*} \quad (8)$$

$$\mathbf{H}_{k+1|k} = [\partial \mathbf{h}_{k+1} / \partial \mathbf{Z}_{k+1}]_{\mathbf{Z}_{k+1}=\hat{\mathbf{Z}}_{k+1|k},\mathbf{f}_{k+1}^*=\hat{\mathbf{f}}_{k|k}^*} \quad (9)$$

$$\mathbf{D}_{k+1|k}^* = [\partial \mathbf{h}_{k+1} / \partial \mathbf{f}_{k+1}^*]_{\mathbf{Z}_{k+1}=\hat{\mathbf{Z}}_{k+1k},\mathbf{f}_{k+1}^*=\hat{\mathbf{f}}_{k|k}^*} \quad (10)$$

Linear forms are obtained, i.e., $\hat{\mathbf{Z}}_{k+1|k+1}$ and $\hat{\mathbf{f}}_{k+1|k+1}^*$ be the estimates of $\mathbf{Z}_{k+1}$ and $\mathbf{f}_{k+1}^*$, respectively, given the observations $(\mathbf{y}_1, \mathbf{y}_2, \ldots, \mathbf{y}_{k+1})$.

3. Mixed artificial algorithm

The overview of methodology can be seen in Fig. 1. Based on the MDP, this model-free method generates an optimal choice when the microgrid system's state and optimal policy at time t are unrelated to their previous states at times t — 1, t — 2, etc. This means that the solution is continuously updated. The topic presented in this article cannot be handled using conventional approaches because most methods require discretizing the action and state space. The effects of dimensionality are something that these solutions have to deal with. As a result of the exponential growth of both the action space and the state space, the complexity of computation and storage is increased. These strategies suffer from the repercussions of dimensionality. The action space and state space grow exponentially, increasing computational and storage complexity. Thus, the typical approaches to controlling energy for the framework of microgrid environment in this work would be difficult to solve by traditional methods. There are several heuristic methods like given in that can solve the optimal EM problem. These methods may not directly address the curse of dimensionality, but they would have low exploration efficiency due to the increasing dimensionality of the search space.

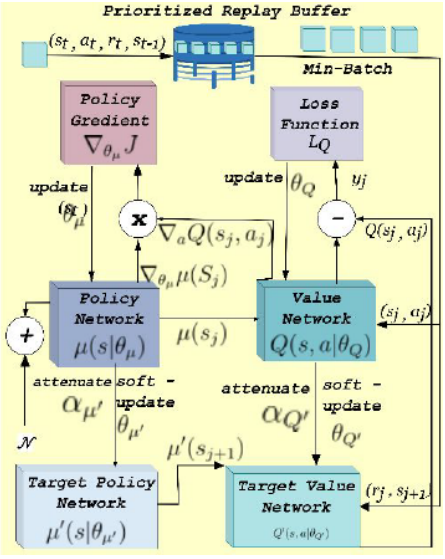

Fig. 1 Deep Deterministic Policy Gradient (DDPG) Agent

The suggested methodology's pseudocode is shown in Algorithm 1. The methodology begins with loading standardized IEEE 33 bus system data, including the electrical network's topology, line, and bus parameters. We install RESs $DG \in \{PV, WT, FC, MT\}$ on specific buses to support generation and increase load demand by adding fast and slow charging stations in the particular buses. A probabilistic model generates the charging station load profile based on a Gaussian distribution to reflect the stochastic nature of charging demands. The microgrid is configured with 10 EV charging stations, integrating the generated load profiles. After adding load and generation, we perform power flow analysis using MATPOWER 7.1 to calculate the power losses in the transmission lines and the voltage levels at different buses. We also incorporate the power balance constraint to verify the fulfilment of demand. Step 3 of Algorithm 1 indicates $total\ generation < Ptdemand$, that if the generation fails to fulfil the demand, the EM strategy becomes necessary otherwise it is unnecessary. To achieve optimal energy management, we train an RL-based DDPG agent to optimize power purchase from RES sources. To train the agent, we define the action variables at as given in Eq. (10), as well as the state variables $st\ cost$, ΔPLoss, and Dt. Subsequently, the agent fulfills the demand by taking appropriate measures. In the event that demand is still unmet, the cost of purchasing power from the power grid is determined. The agent is penalized or rewarded based on the constraints presented in steps vi, xi, xii, and xv of Algorithm 1. As a result, rewarding the agent will result in more positive feedback, preserving the solution, and updating the action in the event of a penalty. The process concludes with the finalization of the optimal energy management strategy and the results will get saved. This advanced strategy ensures the agent learns to make cost-effective and efficient decisions, enhancing the overall performance of the microgrid.

Algorithm. 1: Pseudocode of the proposed methodology

Input: load IEEE 33 bus data, add charging stations Ei, $COSTDG \in \{PV, WT, FC, MT\}$, $COSTGrid$

Output: PDG

t , $Pgrid$

t

1. Generate charging station load profile

2. Run power flow analysis to calculate power loss and system voltage

3. **If** $total\ generation < Pdemand$

t # Check if energy management is required

a. Energy management is required

b. For energy management: train DDPG with a microgrid environment and define extra sources as

action variables at as given in Eq. (10), and define state variable st as cost, change in power loss,

and power deficit represented as $cost$, ΔPLoss, and Dt respectively.

c. For episode = 1:M

i. Add the action at at the MTi, PVi, WTi, FCi

ii. Run power flow analysis

iii. Save the new set of observations through power flow

analysis $st \in [\Delta P\text{Loss}]$

iv. Buy the Dt from the grid

v. Calculate cost and update the states as $st \in [\Delta P\text{Loss}, cost, Dt]$

vi. **If** load demand is matched as given in eq. (6),

1. Give a reward to the agent $rPDemand$

$t = 10$

vii. **else**

2. penalize the agent as given in Eq. (14)

viii. **End**

ix. **If** the voltage limit is violated $V\text{min} > Vj$, $t > V\text{max}$, $\forall j = 1...Nbus$, $\forall t = 1...T$

1. penalize the agent as given in Eq. (14)

x. **else**

2. Give a reward to the agent rVL

$t = 1$

xi. **End**

xii. **If** the power limit of DGs PDG

$i, min \leq PDG$

$it \leq PDG$

i, max as well as grid power limit $Pgrid$

min

$> Pgrid$

$t > P$

$grid$

max is violated,

1. penalize the agent as given in Eq. (14)

xiii. **else**

2. Give a reward to the agent $rPDG$

$it, Pgrid$

t

$t = 10$

xiv. **End**

xv. **If** power loss is greater than the updated loss Pcs

$loss > Pupdated$

$loss$

1. Agent gets rewarded as given in Eq. (13)

xvi. **else**

2. penalize the agent as given in Eq. (14)

xvii. **End**

xviii. Calculate the reward rt

xix. Send feedback to the agent

xx. Update the loss function of DDPG agent from Eq. (18)

xxii. **End**

d. End

4. else

No energy management required

5. End

The total reward for a single simulation, starting at time t with state $s(t)$, is computed as

$$R(s(t), t) = \sum_{k=0}^{M-t} \gamma^k \, r(t+k), \tag{11}$$

The attenuation coefficient [0, 1] represents the degree of reduction in value. The reward for transitioning from state $s\ (t + k - 1)$ to $s\ (t + k)$ with action $a\ (t + k - 1)$ is denoted as $r\ (t + k)$. Then the value function is defined as

$$V\pi\big(s(t)\big) = \mathbb{E}[R(s(t), t) | s\ (t) = s] \tag{12}$$

The agent should discover the best regulation strategy $\pi*$ to optimize $V(s(0),\ 0)$. The agent responsible for managing power distribution is rewarded based on its ability to satisfy specific constraints and reduce power loss compared to the previous state.

$$rt = -|Dt| - 0.01 \times Costt - Penalties \tag{13}$$

$$\begin{aligned} Penalties = &-Power\ Loss\ Penaltyt \\ &-Grid\ Penaltyt - Voltage\ Penaltyt \end{aligned} \tag{14}$$

In order to encourage effective and consistent power management, the reward function is made to incentivise the RL agent to eliminate power deficits, reduce costs, and adhere to grid and voltage constraints. The penalty is defined on the basis of power loss, which is defined in Eq. (3). If the power loss increases from the previous state, the agent will get a penalty. The grid penalty is defined as the agent incurring the power from the grid within a limit. The voltage penalty is defined as the agent's decision to take actions in which the voltage of the system should be within its limit. If the voltage limit is violated, the agent will get a penalty.

Therefore, the subsequent connection is established

$$V\pi(s(0), 0) = \mathbb{E}[OB + Penalties] \tag{15}$$

Then the action of current state st is evaluated using the action value function

$$V^{\pi}\big(s(t)\big) = \max_{a_t \mathcal{U}(s_t)} Q^{\pi}(s, a) \tag{16}$$

$$Q^{\pi}(s, a) = \mathbb{E}_{\pi}\left[\sum_{k=0}^{K} \gamma^k * r_{t+k} | s_t = s;\ a_t = a\right] \tag{17}$$

In this context, the symbol K represents the amount of future time steps taken into account, whereas γ represents a discount factor that determines the balance between immediate and future rewards. Here, the value of γ is set to 1, indicating that DG and grid benefits are considered equally important.

The distribution network environment is manipulated by a learning agent in the DDPG in discrete timesteps, much like in traditional reinforcement learning. Within this framework, the actor and critic components play crucial roles. The actor, parameterized as $\mu\ s \mid \theta\mu$, determines actions based on states deterministically, while the critic $Q(s, a)$ evaluates these actions using the Bellman equation akin to Q-learning principles. The overall performance of critic is updated in accordance with a loss function that has been defined specifically. This integration enables the DDPG algorithm to incorporate EV load profiles and facilitating efficient power purchases from external sources. The update rule for the parameters of the critic is determined by the loss function, as stated in the study in Yu *et al*. (2024).

$$L(\theta^Q) = \frac{1}{B}\Sigma_i\left(y_i - Q(s_i, a_i|\theta^Q)\right)^2 \quad (18)$$

Algorithm 2.

1. Initialize the main actor $\mu\ s \mid \theta\mu$ and critic $Q\ s, a \mid \theta Q$ network
2. Set the parameters of the target actor network μ' and critic network Q'
3. Set up the replay buffer $\mathbb{D}$
4. **For** each episode = 1:Z do
5. Set up $s1$
6. Set up an arbitrary procedure $\mathcal{N}$ for finding the best action
7. **For** t = 1:T do
8. **If** each episode < K then
9. Randomly choose the action at as given in Eq. (10) from the uniform distribution
10. Carry out the selected action at and observe the reward rt as given in Eq. (13) and transfer to the next state $st + 1$
11. Save the change $(at, st, rt, st + 1)$ in reply buffer $\mathbb{D}$
12. **Else**
13. Select action atusing the main actor policy $\mu\ s \mid \theta\mu$ with added exploration noise $\tau * \mathcal{N}t$
14. Implement the at and observe rt as given in Eq. (13) and transfer to the next state st+1
15. Save the change $(at, s1, rt, st + 1)$ in reply buffer $\mathbb{D}$
16. Make a batch of the changes called as minibatch $\mathcal{F} = (aj, sj, rj, sj + 1)\ j = 1$
17. Calculate the target action value $yj = rj + \gamma Q'\ sj + 1, \mu'\ s, a \mid \theta\mu'\ \theta Q'$
18. Update the main critic by minimizing the loss function as given in Eq. (18)
19. Update the main actor network with policy gradient
20. Update the target networks
21. **End if**
22. **End for**

4. Fuzzy criterion for LMI

For an optimization design problem containing inequalities, the mathematical model can be expressed as: finding a set of design variables $\mathbf{X} = (\mathrm{x}_1, \ldots, \mathrm{x}_\mathrm{D})$ to be

$$Minimize\ \mathrm{f}(\mathbf{X})$$
$$Subjectto\ g_j(\mathbf{X}) = \left|\frac{b_j}{(b_a)_j}\right| - 1 \le 0, \quad j = 1 \sim n_n$$
$$\mathrm{x_i} \in \mathrm{S_i},\ \ \mathrm{i} = 1 \sim \mathrm{D}$$

$f(\mathbf{X})$ is the objective function, X is a set of design variables, D is the number of design variables, $g_j(X)$ is the value of the j-th restraint function, n_n is the total number of restraint conditions, b_j is the j-th structural reaction, which can be component stress σ_j, degree of freedom, etc. δ_j, $(\mathrm{b_a})_\mathrm{j}$ and is the j-th structural reaction allowable value.

Moreover, $\mathrm{S_i}$ it is the set of design variables that can be selected. For example, $\mathrm{X_i}$the set of discrete design variables S_i can be expressed as

$$\mathrm{S_i} = \{\mathrm{x_i}(1), \mathrm{x_i}(2), \ldots, \mathrm{x_i}(\mathrm{N})\} \quad (19)$$

In the formula, N is S_i the total number of design variables that can be selected in the discrete set, and $\mathrm{x_i}(\mathrm{k})$ represents S_i the value of the kth selectable design variable in the set. $\mathrm{X_i}$

If $\mathrm{X_i}$ the design variables are continuous, the set S_i can be expressed as follows

$$\mathrm{S_i} = \{\mathrm{x_i} \mid (\mathrm{x_i})_\mathrm{L} \le (\mathrm{x_i}) \le (\mathrm{x_i})_\mathrm{U}\} \quad (20)$$

In the formula $(\mathrm{x_i})_\mathrm{L}$, and $(\mathrm{x_i})_\mathrm{U}$ represent $\mathrm{X_i}$ the upper and lower limits of the design variables respectively. The algorithm was originally used to deal with unconstrained problems. Once a problem with inequality constraints is encountered, the processing method of the fitness function must be redefined to perform generation search. The quality of each solution in the group is determined by the fitness function. Generally, the fitness function is defined according to the characteristics of the problem and is also related to the way the constraint conditions are handled. For solving problems with inequality constraints, the simplest way is to give a weighted combination of the objective function and the constraint function, thus obtaining an unconstrained pseudo-objective function, which is then defined as an adaptation function. The most common way to deal with constraint conditions is the external penalty function method (Chen 2023a). This article chooses the external penalty function method. The individual fitness function is defined as follows (Chen 2023b)

$$\Phi(\mathbf{X}) = \mathrm{f}(\mathbf{X}) + \lambda \sum_{\mathrm{j}=1}^{\mathrm{n_m}} max(0, g_j(X)) \quad (21)$$

where λ is the penalty parameter.

The penalty parameter (λ) is an important parameter that affects the convergence of the hybrid search algorithm. If the penalty parameter is too large, it will lead to premature convergence and the program will fall into the local optimal solution. If it is too small, the penalty will be Multiplying the value of the parameter by the constraint function value will not work, causing the iterated solutions to violate the constraint conditions. For the comprehensive analysis of the static output feedback controller, we use Lyapunov's theorem to analyze its stability, where the Lyapunov function V(x) is expressed as the following form

$$\mathrm{V(x)} = \mathrm{x^T(t)P^{-1}(x)x(t)} \quad (22)$$

Now $0 > \Delta\mathrm{V(x)} - \gamma^2\omega^\mathrm{T}\omega + \mathrm{z^Tz}$, where $\Delta\mathrm{V(x)} = \mathrm{V(x(t+1))} - \mathrm{V(x(t))}$, while $\mathrm{V(x(t+1))} = \mathrm{x^T(t+1)P^{-1}(x^+)x(t+1)}$, $\mathrm{x^+}$ means $\mathrm{x(t+1)}$, then

$$\begin{aligned} 0 &> \mathrm{V(x)} - \gamma^2\omega^T\omega + z^Tz \\ &= x^T(t+1)P^{-1}(x^+)x(t+1) \\ &\quad -x^T(t)P^{-1}(x)x(t) - \gamma^2\omega^T\omega + z^Tz \end{aligned}$$

$$= \begin{bmatrix} x \\ \omega \end{bmatrix}^T \begin{bmatrix} \bar{A}^T_{\mu\mu\mu}(x,y)P^{-1}(x^+) \star -P^{-1}(x) + \bar{C}^T_{\mu\mu\mu}(x,y)\bar{C}^T_{\mu\mu\mu}(x,y) \\ B^T_{\infty\mu}(x)P^{-1}(x^+)\bar{A}_{\mu\mu\mu}(x,y) + D^T_{\infty\mu}(x)\bar{C}_{\mu\mu\mu}(x,y) \\ \bar{A}^T_{\mu\mu\mu}(x,y)P^{-1}(x^+)B_{\infty\mu}(x) + \bar{C}^T_{\mu\mu\mu}(x,y)D_{\infty\mu}(x) \\ B^T_{\infty\mu}(x)P^{-1}(x^+)B_{\infty\mu}(x) + D^T_{\infty\mu}(x)D_{\infty\mu}(x) - \gamma^2 I \end{bmatrix} \begin{bmatrix} x \\ \omega \end{bmatrix}$$

which $\bar{A}^{\mathrm{T}}_{\mu\mu\mu}(\mathrm{x},\mathrm{y})\mathrm{P}^{-1}(\mathrm{x}^+) \star$ means $\bar{A}^{\mathrm{T}}_{\mu\mu\mu}(\mathrm{x},\mathrm{y})\mathrm{P}^{-1}(\mathrm{x}^+)\bar{A}_{\mu\mu\mu}(\mathrm{x},\mathrm{y})$.

When $\mathrm{x} \in \mathrm{R}^{\mathrm{r}}$ a polynomial function f(x) is the sum of squares, it can be expressed as

$$\mathrm{f}(\mathrm{x}) = \sum_{\mathrm{i}=1}^{\mathrm{r}} \mathrm{g}_{\mathrm{i}}^2(\mathrm{x}) \tag{23}$$

where $\mathrm{g}_1(\mathrm{x}) \cdots \mathrm{g}_{\mathrm{t}}(\mathrm{x})$, $\mathrm{g}_2(\mathrm{x})$ is a polynomial function, and a convex polyhedral cone K^{d} constitutes a polynomial $\mathrm{P}^{\mathrm{d}}(\mathrm{x})$, and $\mathrm{P}^{\mathrm{d}}(\mathrm{x})$ conforms to Definition 1, and can be decomposed into a sum of squares, then for all d, $\mathrm{K}^{\mathrm{d}} \subseteq \mathrm{K}^{\mathrm{d}+1}$

$$\mathrm{P}^{\mathrm{d}+1}(\mathrm{x}) = \left(\sum_{\mathrm{k}=1}^{\mathrm{t}} \mathrm{x}_{\mathrm{k}}^2\right) \mathrm{P}^{\mathrm{d}}(\mathrm{x}) = \sum_{\mathrm{k}=1}^{\mathrm{t}} \sum_{\mathrm{i}=1}^{\mathrm{r}} (\mathrm{g}_{\mathrm{i}}\mathrm{x}_{\mathrm{k}})^2. \tag{24}$$

Define a monomial $\mathrm{X} = \mathrm{x}_1^{\alpha_1}\mathrm{x}_2^{\alpha_2} \cdots \mathrm{x}_{\mathrm{r}}^{\alpha_{\mathrm{r}}}$ to the power of α, where $\mathrm{x} \in \mathrm{R}^{\mathrm{r}}$ all $\alpha_{\mathrm{i}}$are non-negative integers, i = 1, 2, ⋯, r and satisfy $\alpha = \alpha_1 + \alpha_2 + \cdots + \alpha_{\mathrm{r}}$.

f(x) is a polynomial function of power 2d, $\mathrm{x} \in \mathrm{R}^{\mathrm{r}}$ and it $\mathrm{Z}(\mathrm{x}) \in \mathrm{R}^{\mathrm{p}}$ is a vector of all monomial combinations of x whose power is not greater than d, then f(x) conforms to definition 1, if and only if there are half positive. The constant matrix $\mathrm{Q} \in \mathrm{S}^{\mathrm{p}}$ satisfies the following equation

$$\mathrm{f}(\mathrm{x}) = \mathrm{Z}^{\mathrm{T}}(\mathrm{x})\mathrm{Q}\mathrm{Z}(\mathrm{x}) \tag{25}$$

The meaning of the above formula is: the square sum polynomial function of the 2d power can always be decomposed into a monomial structure of the d power.

5. Numerical simulation and results

This study used a total of four earthquake durations, including three near-field shock waves JM AKobe, Chi-Chi and JR Takatori, and one far-field shock wave El Centro. The PGA (Peak ground acceleration) value of the near-field shock wave was normalized during analysis. It is 1 g, and the distant shock wave maintains the original shock wave record. Among them, JM AKobe is the north-south surface acceleration record measured at the Kobe Meteorological Agency station of the 1995 Great Hanshin Earthquake in Japan, Chi-Chi is the east-west surface acceleration record measured at the Sun Moon Lake Station of the 1999 Taiwan 921 Earthquake, and JR Takatori is the east-west surface acceleration record measured at the Japan Railway Takatori Station station of the Great Hanshin Earthquake in 1995, and the El Centro shock wave is the north-south surface acceleration record measured at the El Centro Station of the 1940 El Centro Earthquake in California, USA. Each shock wave and its spectrum analysis are shown in Figs. 2 to 5. The main period of JM AKobe is about 0.69 seconds, Chi-Chi is about 0.89 seconds, JR Takatori is about 1.22

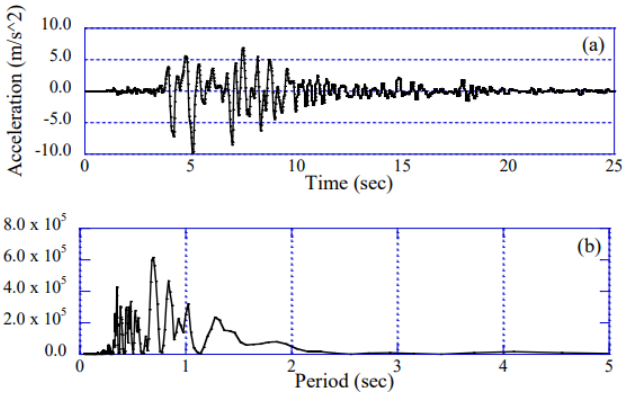

Fig. 2 (a) JMA Kobe surface acceleration record duration chart; (b) JMA Kobe seismic wave spectrum analysis chart

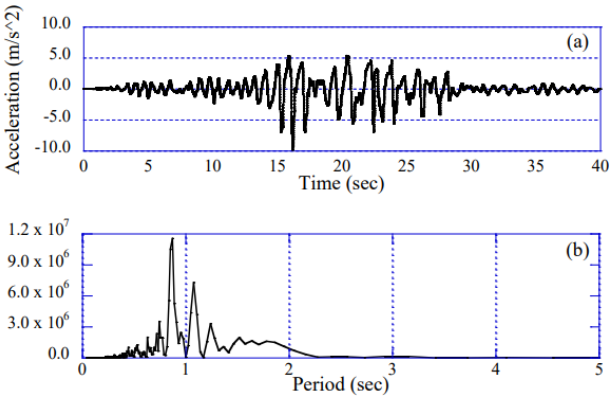

Fig. 3 (a) Chi-Chi surface acceleration record duration chart; (b) Chi-Chi shock wave spectrum analysis chart

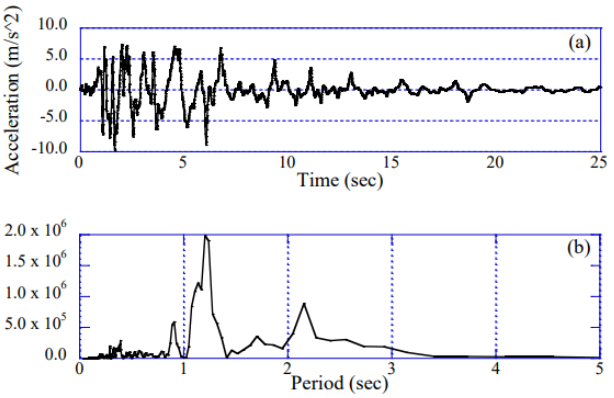

Fig. 4 (a) JR Takatori surface acceleration record duration chart; (b) JR Takatori seismic spectrum analysis chart

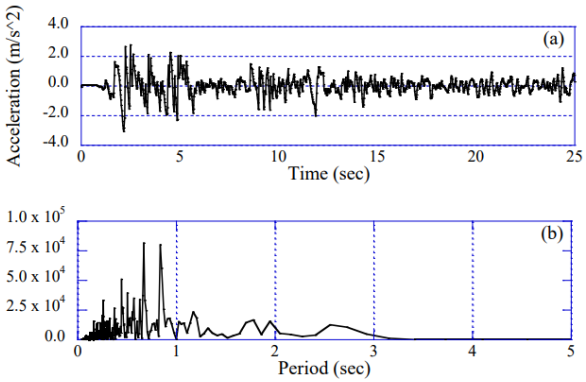

Fig. 5 (a) El Centro surface acceleration record duration chart; (b) El Centro seismic spectrum analysis chart

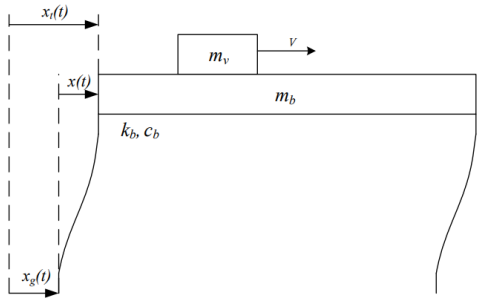

Fig. 6 Schematic diagram of the bridge affected by moving loads and earthquake effects

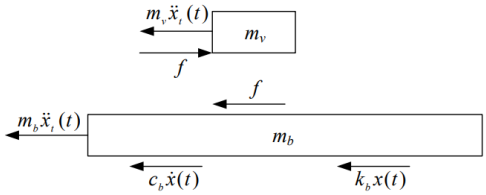

Fig. 7 Free body diagram of bridge and vehicle

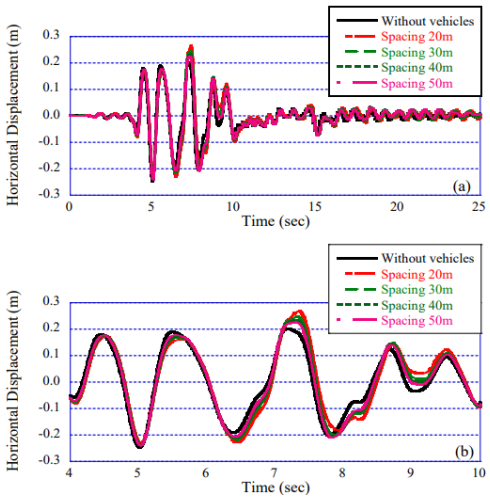

Fig. 8 (a) Horizontal displacement diagram of the bridge deck with different vehicle spacing and no vehicle passing through; (b) Magnified view of bridge deck horizontal displacement for 4-10 seconds

seconds, and El Centro is about 0.68 seconds.

Fig. 5(a) El Centro surface acceleration record duration chart; (b) El Centro seismic spectrum analysis chart

If an earthquake happens to occur when a vehicle passes through a bridge, assuming that the vehicle still travels at a constant speed and does not slide, the schematic diagram of the model is shown in Fig. 6.

m_v is the mass of the car body, m_b is the mass of the bridge superstructure, $x_t(t)$ is the absolute displacement of the bridge deck, $x(t)$ is the relative displacement of the bridge deck, $x_g(t)$ is the surface displacement, k_b and c_b are the stiffness coefficient and damping coefficient of the bridge axial direction respectively. The equation of motion can be expressed as follows

$$m_b\ddot{x}_t(t) + m_v\ddot{x}_t(t) + c_b\dot{x}(t) + k_b x(t) = 0 \tag{26}$$

The force transmitted from the vehicle to the bridge can be known $f = m_v[\ddot{x}_g(t) + \ddot{x}(t)]$ from the free body diagram. Therefore, after shifting the terms of Eq. (26), the bridge motion equation can be obtained

$$\begin{aligned} &m_b\ddot{x}(t) + c_b\dot{x}(t) + k_b x(t) \\ &= -m_b\ddot{x}_g(t) - m_v[\ddot{x}_g(t) + \ddot{x}(t)] \end{aligned} \tag{27}$$

The JMA Kobe seismic acceleration duration record was used in the analysis. The vehicle weighed 72 tons and the driving speed was 100 km/hr. The distance between the front and rear of the vehicle was 20 m, 30 m, 40 m or 50 m respectively, and the traffic flow was uninterrupted. The smaller the distance between the vehicles, the smaller the distance between the vehicles. There are more vehicles at the same time. Fig. 7 is a comparison of the horizontal displacement of the bridge deck with different vehicle spacing and no vehicle passing. From the figure, it can be found that the trends of each curve are roughly the same, and the displacement peak value and difference percentage are listed in Table 1. From Eq. (27), it can be seen that the force of vehicles acting on the bridge is in the opposite direction to the relative acceleration of the bridge deck. Therefore, compared with the example where no vehicle passes, when the distance between vehicles becomes smaller, whether it is a positive displacement peak or a negative displacement peak. The differences are getting bigger. When the distance between vehicles is 40 m or 50 m, the peak value of positive displacement is smaller than the peak value of positive displacement without vehicles. At this time, the peak value of negative displacement is still smaller than the peak value of positive displacement without vehicles. Therefore, the maximum displacement response is smaller than the peak value of positive displacement without vehicles. It was still a small phenomenon.

When no vehicle passes, the bridge pier is still within the linear range, but with traffic passing through, the plastic hinge at the bottom of the bridge pier enters the nonlinear stage, and at the smaller the distance between vehicles, the more obvious it is.

Table 1 Comparison of bridge deck displacement differences between different vehicle spacing and no vehicle passing

	Spacing 20 m	Spacing 30 m	Spacing 40 m	Spacing 50 m	No vehicles
Forward displacement peak value (m)	0.231	0.237	0.240	0.241	0.247
Negative displacement peak value (m)	0.268	0.247	0.235	0.225	0.203
Displacement peak (m)	0.268	0.247	0.240	0.241	0.247
Difference (%)	8.4	0	-3.0	-2.8	-

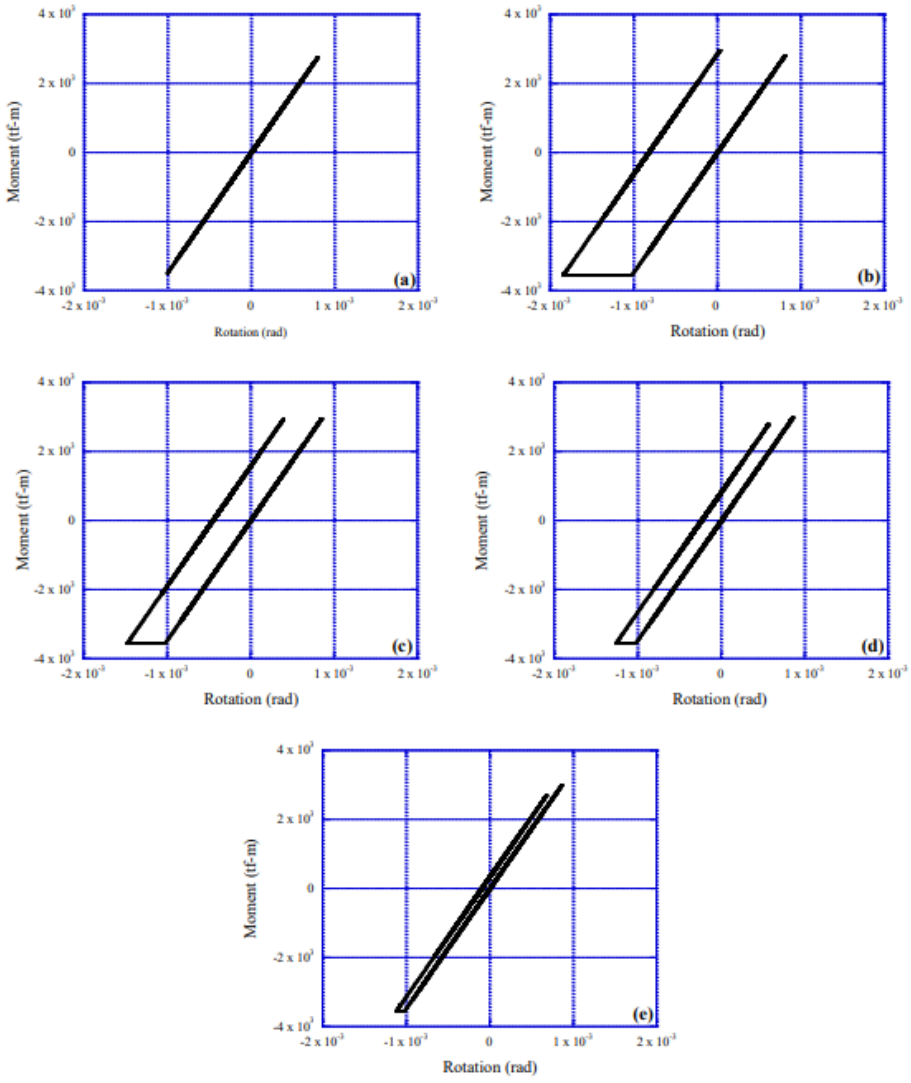

Fig. 9 Bending moment hysteresis loop diagram at the bottom of the bridge pier (a) no vehicle; (b) vehicle spacing 20 m; (c) vehicle spacing 30 m; (d) vehicle spacing 40 m; (e) vehicle spacing 50 m

From the above discussion, it can be known that when an earthquake occurs, if there is a high density of traffic passing through the bridge, after the inertial force of the vehicles is applied to the bridge deck, there will be a chance to amplify the displacement of the bridge deck and cause plasticity at the bottom of the bridge pier. The degree of hinge entry into nonlinearity is even more significant.

First, JMA Kobe seismic wave records were used to compare μthe effect of TMD on reducing the peak horizontal horizontal displacement of the bridge deck when it was between 5% and 100%. The TMD was designed using Hartog's Method introduced in Chapter 3, and the results were analyzed. As shown in Fig. 10. It can be observed from the figure μthat the effect of reducing the peak displacement of the bridge deck is significantly improved when the TMD is equal to 5% and 10% μ. When the TMD is 10%, the bridge deck displacement is reduced by 17.8%. After that, with μ the increase in the displacement peak

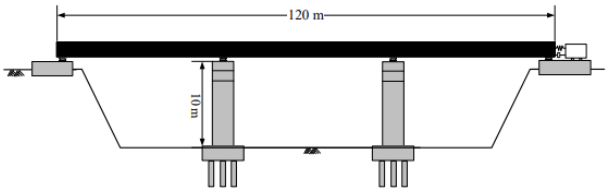

Fig. 10 Schematic diagram of three-span continuous girder bridge and TMD

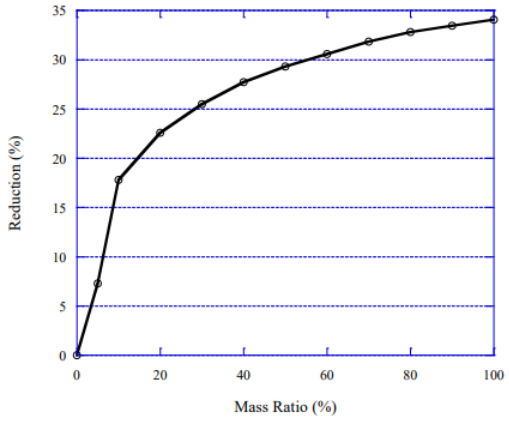

Fig. 11 Displacement reduction percentage curves corresponding to different TMDsμ

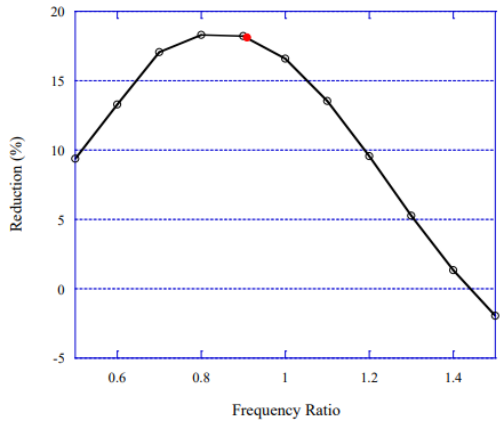

Fig. 12 Displacement peak reduction percentage curve corresponding to different frequency ratios in linear structure (JMA Kobe)

reduction percentage tends to be moderate, and μ the displacement peak value is only reduced by 34.1% at 100%. That is, the TMD mass increases by 10 times, but the displacement reduction percentage only increases by 2 times. It can be seen that when the TMD mass design is too large, it is not economical.

The TMD μ was set to 10%, and the ratio of TMD to the basic natural vibration frequency of the bridge was adjusted to 0.5~1.5. Under different frequency ratios, the corresponding reduction percentage of the peak horizontal displacement of the bridge deck is shown in Figs. 11 to 13. In addition, the frequency ratio (0.909) designed by Hartog's Method is marked with a solid circle in the figure.

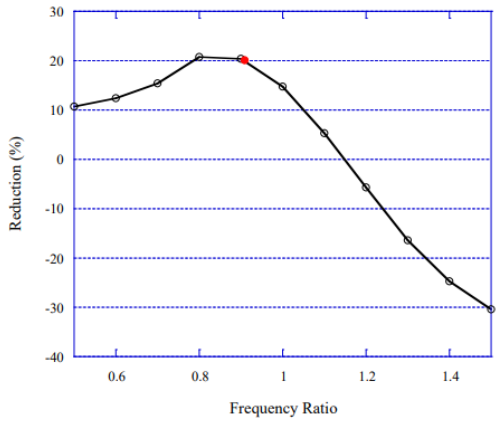

Fig. 13 Displacement peak reduction percentage curve corresponding to different frequency ratios in linear structure (Chi-Chi)

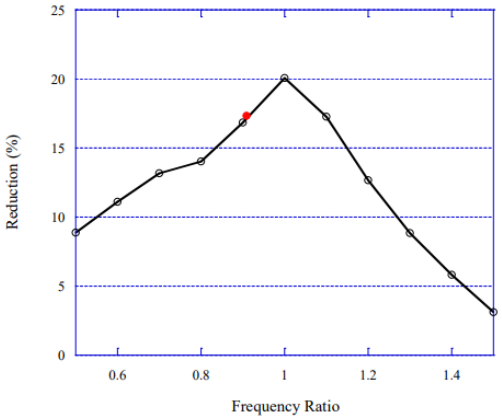

Fig. 14 Displacement peak reduction percentage curve corresponding to different frequency ratios in linear structure (JR Takatori)

The corresponding displacement peak reduction percentages of this design frequency ratio in JMA Kobe, Chi-Chi and JR Takatori are 18.1%, 20.1% and 17.3% respectively. Although it is not the optimal value, it still has a very good vibration reduction effect. When the frequency ratio deviates too much, the vibration reduction effect is significantly reduced. Especially in Chi-Chi shock waves, when the frequency ratio is greater than 1.2, a severe counter-effect occurs. Even when the frequency ratio is 1.5, the displacement peak value is lower than that without TMD installed. The number of bridges increased by 30.43%.

From the percentage reduction curve of the peak displacement of each shock wave and Table 2, it can be seen that the vibration reduction effect of the traditional TMD design method (Hartog's Method) becomes obviously unstable after the structure enters nonlinear behavior, even in Chi-Chi. and El Centro shock waves, whose dynamic analysis results are completely different from the behavior in linear structures. The reason is that after the structure becomes nonlinear, the natural vibration frequency changes. If the TMD still maintains the original design frequency, it will cause the TMD frequency detuning effect and affect its

Table 2 Reduction percentage of peak displacement in different shock waves for TMD (5% and 10%) designed using μHartog's Method under bridge support nonlinearity

	JMA Kobe	Chi-Chi	JR Takatori	El Centro TMD
TMD 5%	7.5	06	3.1	0.4
TMD 10%	12.8	-0.8	5.9	-2.2

displacement control effect. Therefore, the frequency spectrum analysis chart of the output bridge deck displacement under the action of each shock wave is compared with the displacement peak reduction percentage curve chart corresponding to different frequency ratios.

(a) JMA Kobe Shockwave

It can be seen from Fig. 15 that the bridge deck displacement response period reaches an extreme value at 1.42 seconds. In addition, in Fig. 14, under TMD5% and 10%, the displacement peak reduction percentage reaches the extreme value at the frequency ratio of 0.8 (T = 1.06 seconds) and 0.9 (T = 1.2 seconds) respectively, while the frequency ratio is between 0.7 and 1.0 (T = 1.4 seconds to 0.96 seconds) can have good vibration reduction effect.

(b) Chi-Chi Shockwave

Fig. 16 shows the bridge deck displacement peak percentage curve reduced by TMD5% and 10% at different frequency ratios, reaching the maximum value when the frequency ratio is 0.6 (T = 1.59 seconds) and 0.5 (T = 1.91 seconds) respectively. Observing Fig. 17, we can find that the displacement response period has an extreme value at 1.64 seconds, and the period has a considerable response from 1.56 seconds to 1.82 seconds. When the design period of the TMD is within this range, it can most effectively reduce the bridge Panel displacement peak.

(c) JR Takatori Shockwave

In the bridge deck displacement spectrum analysis figure 19, the maximum value appears at the period T = 2.18 seconds, and a peak value also appears at the period T = 1.21 seconds. Therefore, it can be found from Figure 18 that the displacement peak reduction percentage curve also has two peaks. TMD5% and 10% reach the maximum value of the bridge deck displacement peak reduction percentage at the design frequency ratio of 0.4 (T = 2.39 seconds) and 0.5 (T = 1.91 seconds) respectively, while another peak appears at the frequency ratio of 0.8 (T = 1.2 seconds). From the analysis results, it can be observed that the peak period in the bridge deck displacement spectrum analysis is very close to the design period where the TMD effect is better.

(d) El Centro earthquake

In the bridge deck displacement spectrum analysis diagram in Fig. 21, the extreme value appears at the period T = 0.86 seconds, which is very close to the maximum value of the displacement reduction percentage curve in Fig. 20: frequency ratio 1.1 (T = 0.87 seconds). In this example, the design frequency change of TMD is more sensitive to the vibration damping effect. When the frequency ratio increases or decreases slightly, the reduction

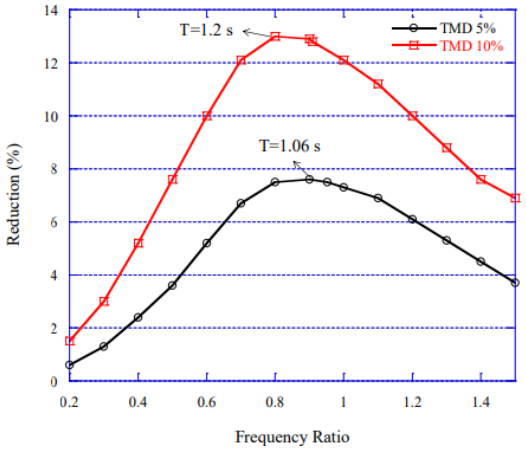

Fig. 15 Displacement peak reduction percentage curve corresponding to bridges with nonlinear supports using TMDs with different frequency ratios (JMA Kobe)

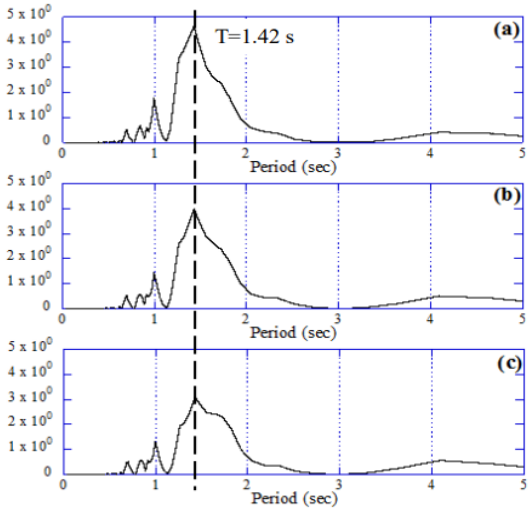

Fig. 16 Bridge deck displacement spectrum analysis chart with nonlinear support (Chi-Chi) (a) No TMD; (b) TMD 5%; (c) TMD 10%

percentage of the displacement peak value decreases significantly.

Based on the above results, it can be seen that after the structure becomes nonlinear, the original TMD design cycle is no longer applicable due to the change of natural vibration frequency. However, according to the dynamic duration analysis results of the bridge, it is known that the TMD design cycle can achieve better vibration reduction effect. It is highly correlated with the period at the peak in the bridge deck displacement spectrum analysis chart. Therefore, in nonlinear structures, the TMD design cycle should be adjusted with reference to the spectrum analysis of structural response in order to achieve better vibration reduction effects.

In addition, observing that the bridge is affected by different earthquake waves, the displacement peak reduction percentage curves corresponding to different frequency ratios of TMD5% and 10% all have the same

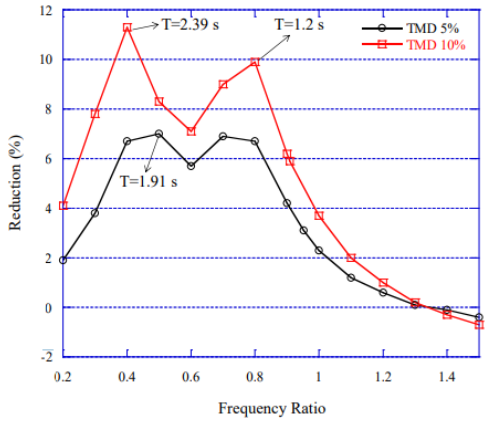

Fig. 17 The displacement peak reduction percentage curve corresponding to the nonlinear support of the bridge using TMD with different frequency ratios (JR Takatori)

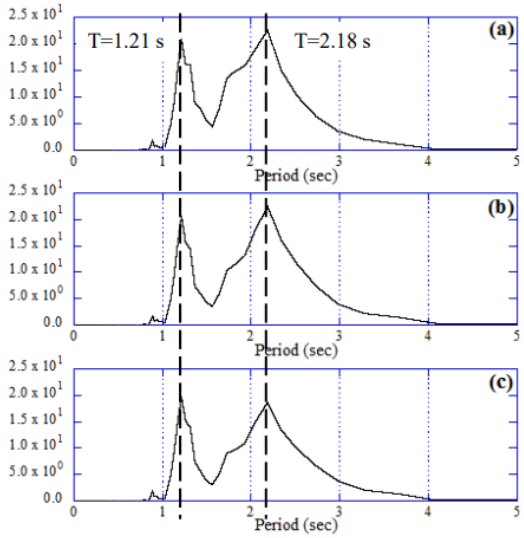

Fig. 18 Bridge deck displacement spectrum analysis chart with nonlinear support (JR Takatori) (a) No TMD; (b) TMD 5%; (c) TMD 10%

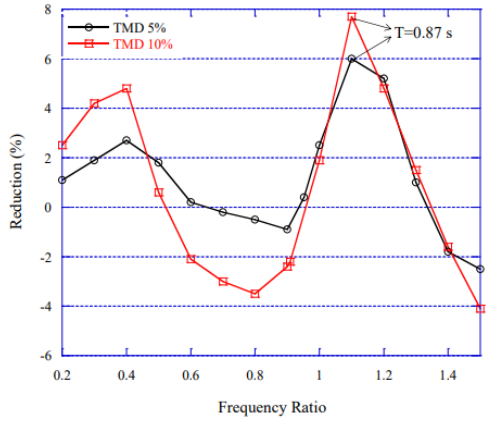

Fig. 19 The displacement peak reduction percentage curve corresponding to the nonlinear support of the bridge using TMD with different frequency ratios (El Centro)

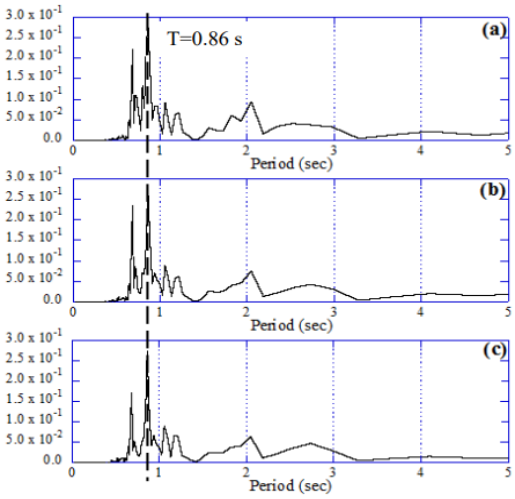

Fig. 20 Bridge deck displacement spectrum analysis chart with nonlinear support (El Centro) (a) No TMD; (b) TMD 5%; (c) TMD 10%

trend. Whether it is a positive effect or a negative effect, μ10% is compared μwith 5%. are more significant, so although choosing a TMD with a larger mass can achieve better vibration reduction effects, if the TMD design frequency is adjusted incorrectly, it will also lead to greater counter-effects. The displacement spectrum connotations of bridges with or without TMD are also quite similar. Figs. 22-23 show the analysis results under the action of JMA Kobe shock waves. From the pier bending moment hysteresis loop, it can be found that the bridge piers still do not yield within the linear range. Therefore, the analysis results are quite similar to Figs. 14 and 15. The optimal vibration reduction is The TMD cycle of the effect remains unchanged.

6. Conclusions

This study has successfully demonstrated the potential of integrating a Smart Lyapunov Linear Matrix Inequality (LMI) criterion with deep reinforcement learning (DRL) algorithms to optimize the performance of tuned mass dampers (TMDs) in reinforced concrete (RC) structures. The findings highlight several key insights and implications for future research and practical applications in structural engineering. Enhanced Seismic Resilience: The proposed framework effectively improves the seismic resilience of RC structures by dynamically adjusting TMD parameters in real-time. The integration of the Smart Lyapunov LMI criterion ensures that the stability of the system is maintained throughout varying seismic conditions, thus providing a robust solution for vibration mitigation. The application of DRL algorithms allows for continuous learning and adaptation of the TMD system based on real-time seismic data. This adaptability is crucial in earthquake-prone regions, where the nature and intensity of seismic events can vary significantly. The use of Lyapunov-based LMIs establishes a solid mathematical foundation for stability analysis. This approach not only facilitates the

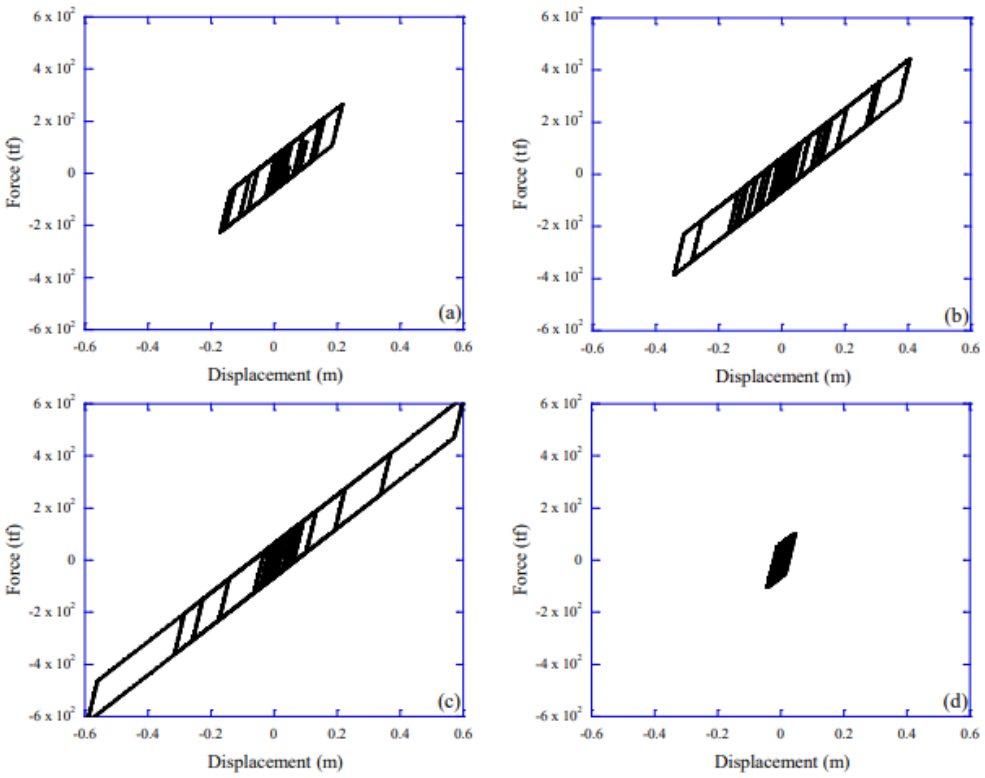

Fig. 21 Hysteresis loop diagram of bridge pier isolation support (a) JMA Kobe; (b) Chi-Chi; (c) JR Takatori; (d) El Centro

design of TMDs but also provides a systematic method for evaluating their effectiveness in different scenarios, ensuring compliance with stability requirements. The combination of Lyapunov stability theory and DRL represents a synergistic approach that leverages the strengths of both methodologies. This innovative framework paves the way for the development of smart structural control systems capable of responding to complex dynamic environments. The findings of this research have significant implications for the design and implementation of TMD systems in RC structures. Engineers and practitioners can utilize the Smart Lyapunov LMI criterion to optimize TMD designs, ensuring that they meet specific performance criteria while maintaining structural integrity. Additionally, the incorporation of DRL algorithms can enhance the operational efficiency of TMDs, allowing for real-time adjustments that improve overall system performance during seismic events. While this study provides a solid foundation for the integration of Smart Lyapunov LMI criteria and DRL in TMD systems, several avenues for future research remain: Future studies should focus on experimental validation of the proposed framework in real-world scenarios. This would provide critical insights into the practical applicability and effectiveness of the system under actual seismic conditions. Exploring the application of the proposed methodology to other types of structural control systems, such as active and semi-active systems, could further enhance its utility in diverse engineering contexts. Investigating the integration of this framework with other emerging technologies, such as IoT sensors and machine learning algorithms, could lead to even more advanced and responsive structural control systems. Research into the long-term performance and durability of TMD systems optimized through this approach will be essential to ensure their reliability and effectiveness over time. In conclusion, the integration of Smart Lyapunov LMI criteria with deep reinforcement learning algorithms represents a significant advancement in the field of structural control. This innovative approach not only enhances the seismic performance of TMD systems in RC structures but also contributes to the development of intelligent, adaptive control strategies that can effectively address the challenges posed by dynamic environmental conditions. As the field continues to evolve, the insights gained from this study will be instrumental in guiding future research and practical applications aimed at improving the resilience of structures in earthquake-prone regions.

Acknowledgments

The authors are grateful for the research grants given to Ruei-Yuan Wang from the Projects of Talents Recruitment of GDUPT, Peoples R China under Grant NO. 2019rc098, and the research grants given to ZY Chen from the Projects of Talents Recruitment of GDUPT (NO. 2021rc002) in Guangdong Province, Peoples R China. as well as to the anonymous reviewers for constructive suggestions.

References

Battista, R.C. and Varela, W.D. (2019), “A system of multiple

controllers for attenuating the dynamic response of multimode floor structures to human walking", *Smart Struct. Syst.*, *Int. J.*, **23**(5), 467-478. https://doi.org/10.12989/sss.2019.23.5.467

Cai, Z., Zhang, T., Jing, X.Y. and Shao, L. (2022a), "Unequal adaptive visual recognition by learning from multi-modal data", *Inform. Sci.*, **600**, 1-21. https://doi.org/10.1016/j.ins.2022.03.076

Cai, Z., Zhang, T., Ma, F. and Jing, X.Y. (2022b), "Dual contrastive universal adaptation network for multi-source visual recognition", *Knowledge-Based Syst.*, **254**, 109632. https://doi.org/10.1016/j.knosys.2022.109632

Chen, C.W. (2023a), "A criterion of robustness intelligent nonlinear control for multiple time-delay systems based on fuzzy Lyapunov methods", *Nonlin. Dyn.*, **76**, 23-31. https://doi.org/10.1007/s11071-013-0869-9

Chen, C.W. (2023b), "Interconnected TS fuzzy technique for nonlinear time-delay structural systems", *Nonlin. Dyn.*, **76**, 13-22. https://doi.org/10.1007/s11071-013-0841-8

Chen, R. (2023c), "A Novel Robotic GWO LDI Modeling and Control for Nonlinear Systems", *Int. J. Acoust. Vib.*, **28**(2). https://doi.org/10.20855/ijav.2023.28.21897

Chen, H., Jing, X.Y., Li, Z., Wu, D., Peng, Y. and Huang, Z. (2020), "An empirical study on heterogeneous defect prediction approaches", *IEEE Transact. Softw. Eng.*, **47**(12), 2803-2822.

Chen, H., Jing, X.Y., Zhou, Y., Li, B. and Xu, B. (2022), "Aligned metric representation based balanced multiset ensemble learning for heterogeneous defect prediction", *Inform. Softw. Technol.*, **147**, 106892. https://doi.org/10.1016/j.infsof.2022.106892

Chen, R., Jing, X.Y., Wu, F., Zheng, W. and Hao, Y. (2023), "Taskspecific parameter decoupling for class incremental learning", *Inform. Sci.*, **651**, p. 119731. https://doi.org/10.1016/j.ins.2023.119731

Chen, H., Huang, B., Zhang, H., Xue, K., Sun, M. and Wu, Z. (2024a), "An efficient Bayesian method with intrusive homotopy surrogate model for stochastic model updating", *Comput.-Aided Civil Infrastr. Eng.*, **39**(16), 2500-2516. https://doi.org/10.1111/mice.13206

Chen, R.S., Zhang, H.Y., Hao, X.K., Yu, H.X., Shi, T., Zhou, H.S., Wang, R.B., Zhao, Z.F. and Wang, P. (2024b), "Experimental study on ultimate bearing capacity of short thin-walled steel tubes reinforced with high-ductility concrete", *Structures*, **68**, p. 107109. https://doi.org/10.1016/j.istruc.2024.107109

Cheng, B., Zhu, D., Zhao, S. and Chen, J. (2016), "Situation-Aware IoT Service Coordination Using the Event-Driven SOA Paradigm", *IEEE Transact. Network Service Manag.*, **13**(2), 349-361. https://doi.org/10.1109/TNSM.2016.2541171

Cheng, L., Jing, X.Y., Zhu, X., Hu, C.H., Gao, G. and Wu, S. (2020), "Local and global aligned spatiotemporal attention network for video-based person re-identification", *Multimedia Tools Appl.*, **79**, 34489-34512. https://doi.org/10.1007/s11042-020-08765-1

Di, M.D. and Magi, F. (2015), "Development of testing methods for endurance trials of composites components", *J. Compos. Mater.*, **49**(24), 2977-2991. https://doi.org/10.1177/0021998314558497

Erum, N. and Ahmad, J. (2023), "Structural, elastic and mechanical properties of cubic perovskite materials", *Arch. Adv. Eng. Sci.*, **2**(1), 24-29. https://doi.org/10.47852/bonviewAAES3202944

Eswaran, M. and Reddy, G.R. (2016), "Numerical simulation of tuned liquid tank–structure systems through sigma-transformation based fluid–structure coupled solver", *Wind Struct.*, *Int. J.*, **23**(5), 421-447. https://doi.org/10.12989/was.2016.23.5.421

Fan, H., Wang, C. and Li, S. (2024), "Novel method for reliability optimization design based on rough set theory and hybrid surrogate model", *Comput. Methods Appl. Mech. Eng.*, **429**, p. 117170. https://doi.org/10.1016/j.cma.2024.117170

Guan, T., Li, B., Song, Y. and Duan, G. (2024), "Fixed-Time Spacecraft Attitude Control With Unwinding-Free Performance", *IEEE Transact. Automat. Control*, 1-8. https://doi.org/10.1109/TAC.2024.3471333

Hao, Y., Jing, X.Y. and Sun, Q. (2022), "Joint learning sample similarity and correlation representation for cancer survival prediction", *BMC Bioinform.*, **23**(1), p. 553.

Huang, H., Yao, Y., Zhang, W. and Zhou, L. (2023), "A push-out test on partially encased composite column with different positions of shear studs", *Eng. Struct.*, **289**, p. 116343. https://doi.org/10.1016/j.engstruct.2023.116343

Huang, H., Chen, Z., Zhao, M., Wang, B. and Ye, Y. (2024), "Seismic performance of frame with middle partially encased composite brace and steel-hollow core partially encased composite spliced frame beam", *J. Build. Eng.*, **95**, p. 110226. https://doi.org/10.1016/j.jobe.2024.110226

Jiang, W., Zheng, B., Sheng, D. and Li, X. (2024), "A compensation approach for magnetic encoder error based on improved deep belief network algorithm", *Sensors Actuat. A: Phys.*, **366**, p. 115003. https://doi.org/10.1016/j.sna.2023.115003

Li, H., Lu, H. and Li, Q. (2024), "Numerical investigations of the influences of valve spool structure on the eccentric jet flow characteristic in high-pressure angle valves", *Energy*, **298**, 131378. https://doi.org/10.1016/j.energy.2024.131378

Lim, S.G. and Hong, C.S. (1989), "Prediction of transverse cracking and stiffness reduction in cross-ply laminated composites", *J. Compos. Mater.*, **23**(7), 695-713. https://doi.org/10.1177/002199838902300704

Lin, L., Liu, J., Huang, N., Li, S. and Zhang, Y. (2024), "Multiscale spatio-temporal feature fusion based non-intrusive appliance load monitoring for multiple industrial industries", *Appl. Soft Comput.*, **167**, p. 112445. https://doi.org/10.1016/j.asoc.2024.112445

Liu, Y., Wang, B., Qian, Z., Yu, J., Shi, T., Fan, Y., Zhou, Y., Ning, Y. and Zhou, X. (2024), "State-of-the art on preparation, performance, and ecological applications of planting concrete", *Case Stud. Constr. Mater.*, **20**, p. e03131. https://doi.org/10.1016/j.cscm.2024.e03131

Long, S., Huang, W., Wang, J., Liu, J., Gu, Y. and Wang, Z. (2024a), "A Fixed-Time Consensus Control With Prescribed Performance for Multi-Agent Systems Under Full-State Constraints", *IEEE Transact. Automat. Sci. Eng.*, 1-10. https://doi.org/10.1109/TASE.2024.3445135

Long, X., Iyela, P.M., Su, Y., Atlaw, M.M. and Kang, S.B. (2024b), "Numerical predictions of progressive collapse in reinforced concrete beam-column sub-assemblages: A focus on 3D multiscale modeling", *Eng. Struct.*, **315**, p. 118485. https://doi.org/10.1016/j.engstruct.2024.118485

Long, X., Li, H., Iyela, P.M. and Kang, S.B. (2024c), "Predicting the bond stress–slip behavior of steel reinforcement in concrete under static and dynamic loadings by finite element, deep learning and analytical methods", *Eng. Fail. Anal.*, **161**, p. 108312. https://doi.org/10.1016/j.engfailanal.2024.108312

Lu, X., Lestari, W. and Hanagud, S. (2001), "Nonlinear vibrations of a delaminated beam", *J. Vib. Control*, **7**(6), 803-831. https://doi.org/10.1177/107754630100700603

Lu, D., Wang, G., Du, X. and Wang, Y. (2017), "A nonlinear dynamic uniaxial strength criterion that considers the ultimate dynamic strength of concrete", *Int. J. Impact Eng.*, **103**, 124-137. https://doi.org/10.1016/j.ijimpeng.2017.01.011

Lu, D., Zhou, X., Du, X. and Wang, G. (2019), "A 3D fractional elastoplastic constitutive model for concrete material", *Int. J. Solids Struct.*, **165**, 160-175. https://doi.org/10.1016/j.ijsolstr.2019.02.004

Meng, Y., Chen, Z.Y., Wang, R.Y., Peng, S.H., Yang, Y. and Chen, T. (2022), "Dynamic intelligent control of composite buildings

by using M-TMD", *Steel Compos. Struct., Int. J.*, **42**(5), 591-598. https://doi.org/10.12989/scs.2022.42.5.591

Meng, S., Zhang, C., Shi, Q., Chen, Z., Hu, W. and Lu, F. (2023), "A robust infrared small target detection method jointing multiple information and noise prediction: Algorithm and benchmark", *IEEE Transact. Geosci. Remote Sens.*, **61**, 1-17. https://doi.org/10.1109/TGRS.2023.3295932

Meng, W., Xin, L., Jinshuai, S., Weiwei, L., Zhongzheng, F., Shuai, W., Jiaxu, K. and Wenguang, Y. (2024), "A study on the reasonable width of narrow coal pillars in the section of hard primary roof hewing along the air excavation roadway", *Energy Sci. Eng.*, **12**(6), 2746-2765. https://doi.org/10.1002/ese3.1799

Ni, L., Chen, J., Chen, G., Zhao, D., Wang, G. and Aphale, S.S. (2024), "An explainable neural network integrating Jiles-Atherton and nonlinear auto-regressive exogenous models for modeling universal hysteresis", *Eng. Applicat. Artif. Intell.*, **136**, p. 108904. https://doi.org/10.1016/j.engappai.2024.108904

Niu, J., Li, Z., Chen, H., Dong, X. and Jing, X.Y. (2022), "Data sampling and kernel manifold discriminant alignment for mixed-project heterogeneous defect prediction", *Softw. Quality J.*, **30**(4), 917-951. https://doi.org/10.1007/s11219-022-09588-z/

Poudel, Y.K. and Bhandari, P. (2023), "Control of the BLDC Motor Using Ant Colony Optimization Algorithm for Tuning PID Parameters", *Arch. Adv. Eng. Sci.*, **2**(2), 108-113. https://doi.org/10.47852/bonviewAAES32021184

Preumont, A. (2011), *Vibration Control of Active Structures: An Introduction*, Springer.

Rabiei, K., Ordokhani, Y. and Babolian, E. (2017), "The Boubaker polynomials and their application to solve fractional optimal control problems". *Nonlinear Dynamics*, **88**(2), 1013-1026. https://doi.org/10.1007/s11071-013-0841-8

Shen, J., Sheng, H., Wang, S., Cong, R., Yang, D. and Zhang, Y. (2023), "Blockchain-based distributed multi-agent reinforcement learning for collaborative multi-object tracking framework", *IEEE Transact. Comput.* https://doi.org/10.1109/TC.2023.3343102

Shi, M., Lv, L. and Xu, L. (2023), "A multi-fidelity surrogate model based on extreme support vector regression: fusing different fidelity data for engineering design", *Eng. Computat.*, **40**(2), 473-493. https://doi.org/10.1108/EC-10-2021-0583

Shu, J., Yu, H., Liu, G., Duan, Y., Hu, H. and Zhang, H. (2025), "DF-CDM: Conditional diffusion model with data fusion for structural dynamic response reconstruction", *Mech. Syst. Signal Process.*, **222**, p. 111783. https://doi.org/10.1016/j.ymssp.2024.111783

Tan, J., Zhang, K., Li, B. and Wu, A. (2023), "Event-Triggered Sliding Mode Control for Spacecraft Reorientation With Multiple Attitude Constraints", *IEEE Transact. Aerosp. Electron. Syst.*, **59**(5), 6031-6043. https://doi.org/10.1109/TAES.2023.3270391

Tian, G., Tan, J., Li, B. and Duan, G. (2024), "Optimal fully actuated system approach-based trajectory tracking control for robot manipulators", *IEEE Transact. Cybernet.*, 1-10. https://doi.org/10.1109/TCYB.2024.3467386

Toma, S. and Chen, W.F. (2024), "A Study on Safety Criteria for Toppling of Pile Drivers and Cranes Based on Structural Stability", *Arch. Adv. Eng. Sci.*, 1-7. https://doi.org/10.47852/bonviewAAES42022138

Tsai, P.W., Hayat, T., Ahmad, B. and Chen, C.W. (2015), "Structural system simulation and control via NN based fuzzy model", *Struct. Eng. Mech., Int. J.*, **56**(3), 385-407. https://doi.org/10.12989/sem.2015.56.3.385

Wang, J., Lin, S.Q., Tan, D.Y., Yin, J.H., Zhu, H.H. and Kuok, S.C. (2024a), "A Novel Method for Integrity Assessment of Soil-Nailing Works with Actively Heated Fiber-Optic Sensors", *J. Geotech. Geoenviron. Eng.*, **150**(8), p. 04024063. https://doi.org/10.1061/JGGEFK.GTENG-11790

Wang, J., Wu, Y., Chen, C.L.P., Liu, Z. and Wu, W. (2024b), "Adaptive PI event-triggered control for MIMO nonlinear systems with input delay", *Inform. Sci.*, **677**, p. 120817. https://doi.org/10.1016/j.ins.2024.120817

Wang, S., Lin, S. and Yang, R. (2024c), "A lightweight convolutional neural network for multipoint displacement measurements on bridge structures", *Nonlinear Dyn.*, **112**(14), 11745-11763. https://doi.org/10.1007/s11071-024-09673-x

Wang, M., Kang, J., Liu, W., Li, M., Su, J., Fang, Z., Li, X., Shang, L., Zhang, F. and Guo, C. (2024d), "Design and study of mine silo drainage method based on fuzzy control and Avoiding Peak Filling Valley strategy", *Scient. Reports*, **14**(1), p. 9300. https://doi.org/10.1038/s41598-024-60228-x

Wang, M., Su, J., Qin, H., Shang, L., Kang, J., Liu, W., Li, M., Zhang, F., Li, X. and Fang, Z. (2024e), "Research on Active Advanced Support Technology of Backfilling and Mining Face", *Rock Mech. Rock Eng.*, **57**(9), 7623-7642. https://doi.org/10.1007/s00603-024-03808-7

Wu, M., Tian, W., He, J., Liu, F. and Yang, J. (2023), "Seismic isolation effect of rubber-sand mixture cushion under different site classes based on a simplified analysis model", *Soil Dyn. Earthq. Eng.*, **166**, p. 107738. https://doi.org/10.1016/j.soildyn.2022.107738

Xu, B. and Guo, Y. (2022), "A novel DVL calibration method based on robust invariant extended Kalman filter", *IEEE Transact. Vehicular Technol.*, **71**(9), 9422-9434. https://doi.org/10.1109/TVT.2022.3182017

Xu, B., Wang, X., Zhang, J., Guo, Y. and Razzaqi, A.A. (2022), "A novel adaptive filtering for cooperative localization under compass failure and non-gaussian noise", *IEEE Transact. Vehicular Technol.*, **71**(4), 3737-3749. https://doi.org/10.1109/TVT.2022.3145095

Yao, Y., Huang, H., Zhang, W., Ye, Y., Xin, L. and Liu, Y. (2022), "Seismic performance of steel-PEC spliced frame beam", *J. Constr. Steel Res.*, **197**, p. 107456. https://doi.org/10.1016/j.jcsr.2022.107456

Ying, Z.G., Ni, Y.Q. and Duan, Y.F. (2019), "Stochastic stability control analysis of an inclined stay cable under random and periodic support motion excitations", *Smart Struct. Syst., Int. J.*, **23**(6), 641-651. https://doi.org/10.12989/sss.2019.23.6.641

Yu, S., Guan, D., Gu, Z., Guo, J., Liu, Z. and Liu, Y. (2024), "Radar Target Complex High-Resolution Range Profile Modulation by External Time Coding Metasurface", *IEEE Transact. Microw. Theory Techniq.*, **72**(10), 6083-6093. https://doi.org/10.1109/TMTT.2024.3385421

Zhang, C. (2023), "The active rotary inertia driver system for flutter vibration control of bridges and various promising applications", *Sci. China Technol. Sci.*, **66**(2), 390-405. https://doi.org/10.1007/s11431-022-2228-0

Zhang, X., Li, S., Jing, X.Y., Ma, F. and Zhu, C. (2020), "Unsupervised domain adaption for image-to-video person reidentification", *Multimedia Tools Appl.*, **79**, 33793-33810. https://doi.org/10.1007/s11042-019-08550-9

Zhang, C., Duan, C. and Sun, L. (2024a), "Inter-storey isolation versus base isolation using friction pendulum systems", *Int. J. Struct. Stabil. Dyn.*, **24**(02), p. 2450022. https://doi.org/10.1142/S0219455424500226

Zhang, W., Lin, J., Huang, Y., Lin, B. and Liu, X. (2024b), "Experimental and numerical studies on flexural performance of composite beams under cyclic loading", *Structures*, **70**, p. 107728. https://doi.org/10.1016/j.istruc.2024.107728

Zhang, X., Hou, D., Xiong, Z., Liu, Y., Wang, S. and Li, Y. (2024c), "EALLR: Energy-Aware Low-Latency Routing Data Driven Model in Mobile Edge Computing", *IEEE Transact. Consum. Electron.* https://doi.org/10.1109/TCE.2024.3507158

Zheng, C., An, Y., Wang, Z., Wu, H., Qin, X., Eynard, B. and Zhang, Y. (2022), "Hybrid offline programming method for

robotic welding systems", *Robot*. *Comput*.-*Integr*. *Manuf*., **73**, p. 102238. https://doi.org/10.1016/j.rcim.2021.102238

Zheng, C., An, Y., Wang, Z., Qin, X., Eynard, B., Bricogne, M., Le Duigou, J. and Zhang, Y. (2023), "Knowledge-based engineering approach for defining robotic manufacturing system architectures", *Int*. *J*. *Product*. *Res*., **61**(5), 1436-1454. https://doi.org/10.1080/00207543.2022.2037025

Zhou, X., Lu, D., Du, X., Wang, G. and Meng, F. (2020), "A 3D non-orthogonal plastic damage model for concrete", *Comput*. *Methods Appl*. *Mech*. *Eng*., **360**, p. 112716. https://doi.org/10.1016/j.cma.2019.112716

Zhu, C., Li, X., Leung, V.C., Yang, L.T., Ngai, E.C.H. and Shu, L. (2017), "Towards pricing for sensor-cloud", *IEEE Transact*. *Cloud Comput*., **8**(4), 1018-1029. https://doi.org/10.1109/TCC.2017.2649525

Zhu, D., Ma, Y., Li, X., Fan, L., Tang, B. and Kang, Y. (2024a), "Transient stability analysis and damping enhanced control of grid-forming wind turbines considering current saturation procedure", *IEEE Transact*. *Energy Convers*., 1-11. https://doi.org/10.1109/TEC.2024.3442925

Zhu, D., Wang, Z., Ma, Y., Hu, J., Zou, X. and Kang, Y. (2024b), "Hybrid LVRT control of doubly-fed variable speed pumped storage to shorten crowbar operational duration", *IEEE Transact*. *Power Electron*., **39**(11), 14192-14203. https://doi.org/10.1109/TPEL.2024.3435063